C: Energy Conversion and Storage; Energy and Charge Transport

Enhancing the Detonation Properties of Liquid Nitromethane by Adding Nitro-Rich Molecule Nitryl Cyanide

Dezhou Guo, Sergey V. Zybin, William A. Goddard, and Qi An

J. Phys. Chem. C, **Just Accepted Manuscript** • DOI: 10.1021/acs.jpcc.0c02010 • Publication Date (Web): 10 Apr 2020

Enhancing the Detonation Properties of Liquid Nitromethane by Adding Nitro-Rich Molecule Nitryl Cyanide

AUTHOR NAMES

Dezhou Guo[1], Sergey V. Zybin[2], William A. Goddard III[2], and Qi An[1*]*

AUTHOR ADDRESS

[1]Department of Chemical and Materials Engineering, University of Nevada-Reno, Reno, Nevada 89557, USA

[2]Materials and Process Simulation Center, California Institute of Technology, Pasadena, California 91125, United States

Corresponding authors: *Email: qia@unr.edu; wag@caltech.edu

ABSTRACT

Nitromethane (NM) is widely used in a variety of industrial applications because of its simple molecular structure and its good combustion and detonation properties. We propose to improve the detonation properties of NM by mixing with the recent synthesized $NCNO_2$ molecule. We used both ReaxFF reactive molecular dynamics (RMD) and quantum mechanics molecular dynamics (QMMD) to investigate the detonation properties. We find that the 1:1 mixture significantly improve detonation properties including Chapman-Jouguet (CJ) temperature, CJ pressure, and detonation velocity. This is because the number of nitrogen atoms increases the gaseous final products while producing fewer carbon clusters. The detonation properties are also enhanced by the increased initial density leading to higher gas expansion capability. Thus, $NCNO_2$ is a good additive to NM or a suitable replacement for liquid NM due to its simple molecular structure, huge energy release, and excellent detonation performance under low temperature conditions.

1. INTRODUCTION

Nitromethane (NM), the simplest organic nitro compound, is widely used in a variety of industrial applications, such as pharma, solvent, fiber, and coating engineering. An important application of NM is as a fuel additive in combustion engines since it is a flammable liquid under ambient conditions[1]. Under shock compression, NM becomes highly sensitive and easily triggered to detonate, making it a representative candidate to understand the shock-to-detonation transition in condensed-phase high energy density materials (HEDM)[2]. During detonation, NM first experiences a highly non-stationary overdriven detonation condition, and then decays towards a steady detonation[3]. For several decades, many studies of NM detonation have been framed in terms of a classical homogeneous model. For example, Travis *et al.* pointed out that chemical reactions initiate *before* the super detonation[4]. Nunziato *et al.* showed that the reaction rates of NM depend on temperature through two different Arrhenius kinetics laws[5]. Kapila *et al.* investigated the gaseous systems and found that the super detonation develops gradually by an initial weak detonation[6]. Yoo *et al*. classified the shock-induced chemical reaction processes in terms of three steps[7]:

1. first is an unreactive induction period,
2. this is followed by a shock initiated chemical reactions period, which
3. finally turns into a rapid exothermic reactions period.

Although these studies provided theoretical and experimental insights into the nature of NM detonation phenomena, the fast and complex atomic processes occurring during detonation for condensed phases remain unknown.

It is known that the detonation properties of NM can be significantly affected by additives. For example, the addition of 2% (by weight) of diethylenetriamine $(CH_2CH_2NH_2)_2NH$ (DETA) reduces the detonation pressure from 10.0 GPa to 7.5 GPa[8]. In addition, micron-sized silica particles change the initiation physical properties of NM from homogeneity to heterogeneity, changing the detonation properties[9]. These phenomena occur because impurities lead to easily formed active species that can sharply increase initial reaction rates.

Recently, nitryl cyanide ($NCNO_2$) was successfully synthesized[10], that contains a strong oxidizer (NO_2 group) adjacent to an excellent fuel (CN group). This new material is expected to be a promising liquid energetic material for propellent and other related applications because of its simple molecular structure with no hydrogen atoms. It includes 38.9% nitrogen element (by weight), much higher than the 18.7% of NM. Thus, we expect that adding $NCNO_2$ to NM may significantly enhance detonation properties.

The kinetic and energetic behaviors of EMs during heating are greatly influenced by their densities. This is because increased denser materials lead to more frequent and effective collisions among molecules at normal pressure conditions. Thus, Zhang *et al*. investigated the decomposition mechanism of 1,3,5-triamino-2,4,6-trinitrobenzene (TATB) and octahydro-1,3,5,7-tetranitro-1,3,5,7-tetrazocine (HMX), and found that high density influences the endothermic reaction pathway that absorbs external energy[11]. Rom *et al*. found that the rate-determining step for the thermal decomposition of NM at normal density is quite different than at high densities. Unimolecular C-N bond cleavage is the first event during heating at ambient condition, whereas at compressed conditions, bimolecular reactions of NM becomes dominant[12]. Thus, we expect that the detonation properties of NM will be influenced by changing its initial densities.

In this paper, we use a combination of reactive force field molecular dynamics (RMD) with quantum mechanics molecular dynamics (QMMD) to predict the thermodynamic parameters of the Chapman-Jouguet (CJ) state to indicate the change in detonation performance[13, 14] of NM from combining with $NCNO_2$. First, we predicted the detonation pressure, detonation temperature and detonation velocity of liquid NM, which we found to be consistent with experimental measurements. Then we predicted the detonation products, which include the dominant products of N_2, H_2O, CO, CO_2 and carbon clusters. Next, we examined the enhanced detonation properties of NM from adding $NCNO_2$. We found that the detonation properties are significantly improved suggesting that $NCNO_2$ is a promising additive or a suitable replacement of liquid NM under low temperature conditions. This study provides a useful approach to develop high performance liquid energetic materials for civil and military applications.

2. SIMULATION METHODS

2.1 Simulation Models

Both NM and $NCNO_2$ are liquid phase at 273 K, therefore, we built the liquid models by randomly distributing molecules in a cubic supercell. We first built a pure NM system with 12 molecules with the cell length of a = b = c = 9.78 Å, leading to the experimental density of 1.14 g/cm^3 at room temperature. Then we replaced 6 NM molecule with 6 $NCNO_2$ molecules to make the mixture. We then optimized the structure using density functional theory (DFT). Then, we heated up the geometry optimized cells to 273 K using QMMD and adjusted the cell lengths until the inner pressure to ~1 atmosphere. Then we performed 20 ps simulations to equilibrate the system. We predict an equilibrium density of liquid NM to be 1.20 g/cm^3, agreeing well with the experimental values of 1.14 g/cm^3 at ambient conditions. We predict that the equilibrium density of the mixture system is 1.38 g/cm^3 at 273 K. The radial distribution function of the mixed system,

displayed in Fig S1 of Supporting Information (SI), exhibits a typical liquid character, indicating that $NCNO_2$ molecules are fully dissolved in the NM. We also compressed pure NM by 15% volume, to obtain a density of 1.38 g/cm^3, so that we could investigate the effect of density on the detonation properties of NM. The compressed system was optimized and heated up to 273 K using the same procedure as pure NM, leading to an initial pressure of 1.48 GPa. The optimized structures at 0 K are shown in Figure 1.

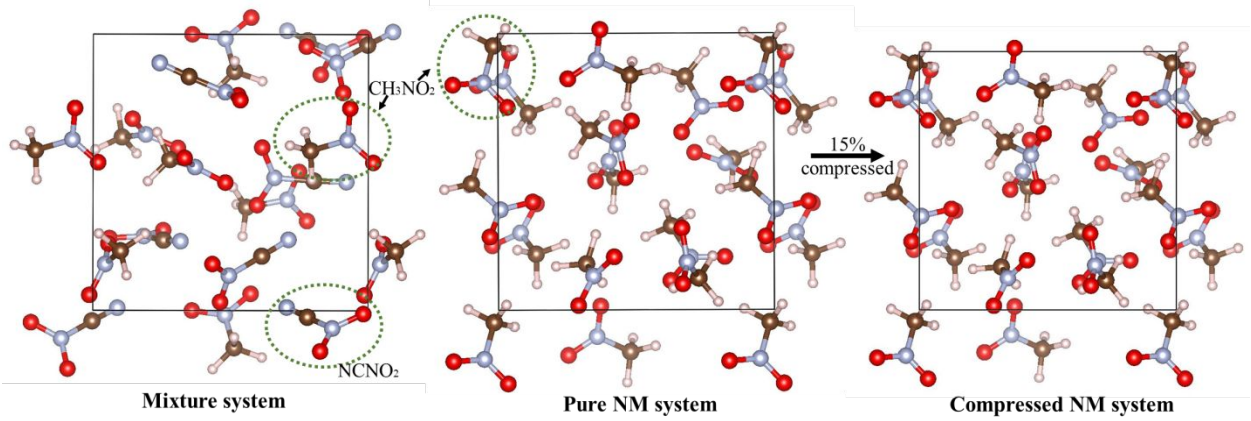

Figure 1. Liquid structure of mixture (left), pure NM (middle) and compressed NM (right) systems at 0 K. The C, N, O, H atoms are represented by brown, light blue, red, and white balls, respectively. The structures are plotted using VESTA visualization software[15].

The structure optimization and equilibrium dynamics were performed using the density functional theory (DFT) and QMMD, respectively, implementation in VASP with plane wave basis set[16,17]. We used the Perdew-Burke-Ernzerh (PBE) functional with the van der Waals interactions described using the D3 method with Becke-Jonson damping parameters[18]. We used the projector augmented-wave (PAW) method for the exchange-correlation interaction and the core-valence interaction, respectively[19,20]. These PAW pseudopotentials consider the 1*s* electrons of C, N, O as the core. The tetrahedron method with Blöchl corrections was applied to determine the electron partial occupancies[21].

The kinetic energy cutoff was set to 500 eV for the plane wave expansions. The energy and force convergence criteria were set to a 1×10^{-5} eV and 1×10^{-2} eV·Å^{-1} for the electronic self-consistent field (SCF) procedure and ionic relaxation loop, respectively. The Brillouin zone integration was performed on Γ-centered symmetry-reduced Monkhorst−Pack meshes with 1×1×1 k-point grid mesh.

2.2 Method to Predict Chapman-Jouguet State

Detonation propagates with a leading shock wave that compresses the reactive medium materials followed by an exothermic reaction zone just behind the shock front containing very complex physical states and chemical reactions evolving under extreme conditions of high temperatures and pressures. Based on the Zeldovich-von Neumann-Döring (ZND) detonation model and the Chapman-Jouguet (CJ) theory, the CJ state describes the key chemical equilibrium state of the products at the end of the reaction zone of the detonation wave for sustained detonation. The Hugoniot equation can be obtained by considering the conservation law of mass, momentum, and energy before and after a detonation wave as:

$$H = e - e_0 - \frac{1}{2}(p + p_0)(v_0 - v)=0 \quad (1)$$

where p is the pressure, e is the specific internal energy, and v is the specific volume. The term "specific" refers to the quantity per unit mass, while the subscript "*0*" refers to the quantity in the initial un-shocked state.

This Hugoniot equation contains two independent variables of pressure and density[22,23]. After a series of rapid chemical energy release processes, all the theoretically possible states of the detonation products can be described by the fully reacted Hugoniot (H=0) curve. Here we located five H=0 points using quadratic polynomial fitting to describe the Hugoniot curve accurately, as

suggested in previous studies[13]. To obtain the various volume-compression-ratios V/V_0, we compressed the initial system at room temperature to five different V/V_0 ratios using strain rates of 4%/ps. Then the systems were equilibrated at these V/V_0 ratios for 5 ps. Finally, we performed cookoff simulations to heat these five compressed systems to five high temperatures to locate the five H=0 points. In addition, the Hugoniot equation was related to the thermodynamic properties between inert and detonated states. The equilibrium properties of the inert state were obtained by averaging the last 10 ps of QMMD based NVT simulations (constant temperature, constant volume and constant number of particles) at normal conditions. For the final reacted states, we carried out ~200 ps of reactive molecular dynamics (RMD) simulation until equilibrated followed by additional 30 ps QMMD simulation. The parameters for the final reacted states were determined by averaging the last 10 ps of QMMD simulations. The properties of the detonated states were calculated by two steps: RMD simulations are first carried out at specific temperatures and densities for hundreds of picoseconds to obtain the full reacted states; then the final RMD output (the atom positions and velocities) are inputted into QMMD simulations for accurate descriptions. This provides a practical way to reach the CJ state with moderate computational costs, allowing the detailed physical and chemical information at the CJ state to be outputted directly without any prior assumptions about the chemical distribution. The CJ point is the tangent point between the detonated Hugoniot curve and the Rayleigh line subjected to the sustained shock wave. The Hugoniot curve is fitted in quadratic polynomial form. Thus, CJ state points can be located on the pressure-volume plane.

The detonation velocity D_{CJ} can be calculated as:

$$D_{CJ} = \sqrt{\frac{P_{CJ} - P_0}{\rho_0(1 - \frac{V_{CJ}}{V_0})}} \qquad (2).$$

Similarly, the CJ temperature (T_{CJ}) can be obtained using V_{CJ}/V_0 in the functional form of the $T \sim V/V_0$ curve.

We performed the RMD simulations using the large-scale atomic/molecular massively parallel simulator (LAMMPS) code[24] (Plimpton et al., 1995). We used a time step as 0.1 fs with periodic boundary condition along three dimensions to avoid surface effect. We used the ReaxFF-lg force field[25], which leads accuracy close to density functional theory (DFT), but with much lower computational cost[26,27]. ReaxFF enables simulation of thermal decomposition of energetic materials with multiple intermediates during for hundreds of picoseconds. Rather than using bond distance, the bond orders are used to construct a connectivity matrix to analyze the molecular fragments in the QMMD simulations. The atomic coordinates for each snapshot from QMMD were extracted and used as input coordinates for ReaxFF-lg simulations implemented in LAMMPS. Then, the bond orders were computed using the bond-order-bond-distance relationship in ReaxFF-lg based on these atomic coordinates. Finally, the detailed products information is obtained by the molecular analytical procedure using the connectivity matrix. The bond order cutoff of 0.3 was applied to identify the independent molecules. Fake bonds from transient bond breaking and formation due to thermal fluctuations were avoided by using time window. Two different time windows (1ps and 2ps) are tested and the time window of 1 ps is good enough to avoid all possible fake bonds.

3 RESULTS AND DISCUSSION

In order to locate the detonated Hugoniot states, we performed a series of long cook-off simulations at prescribed temperatures and volume compression rates. The range of temperatures

and volume-compressions must meet the requirement that the final Hugoniot values are close to zero. Thus, we considered five sets of temperatures and five different densities for each temperature using the ReaxFF force field. The canonical (NVT) ensemble was applied to control the temperature with a damping constant of 100 fs. The thermal coupling between the system and thermostat is 100 fs which is much longer than the timescale of bond broken and formation. Figure 2 shows the time evolutions of total energy at $V/V_0 = 0.65$ with $T = 3400$ K for NM, and at $V/V_0 = 0.65$ with $T = 4700$ K for the mixture system, respectively.

The energy evolution illustrates the degree of thermal decomposition. The total energy initially increases slightly in the endothermic stage of decomposition, and then decreases rapidly in the transition to the exothermic stage in which secondary reactions release energy to form stable product molecules, as shown in Figure 2 (a, c). This transition occurs earlier with increased temperatures. After the exothermic period, the energy decreases slowly as the system gradually reaches an equilibrium steady state, which is further verified by the extra 100 ps simulation. Next, the atom positions and velocities at the very end of RMD simulations are extracted as inputs for QMMD simulations of additional 30 ps to obtain an accurate first-principles description, as shown in Figure 2 (b, d). During the 30 ps QMMD simulation, the total energy fluctuates around a constant value and the stable products (H_2O, CO_2, N_2, CO and *etc*.) remain dynamically stabilized for the last 10 ps. Thus, the properties of fully decomposed states, such as pressure and total energy, are determined by averaging the last 10 ps QMMD simulations.

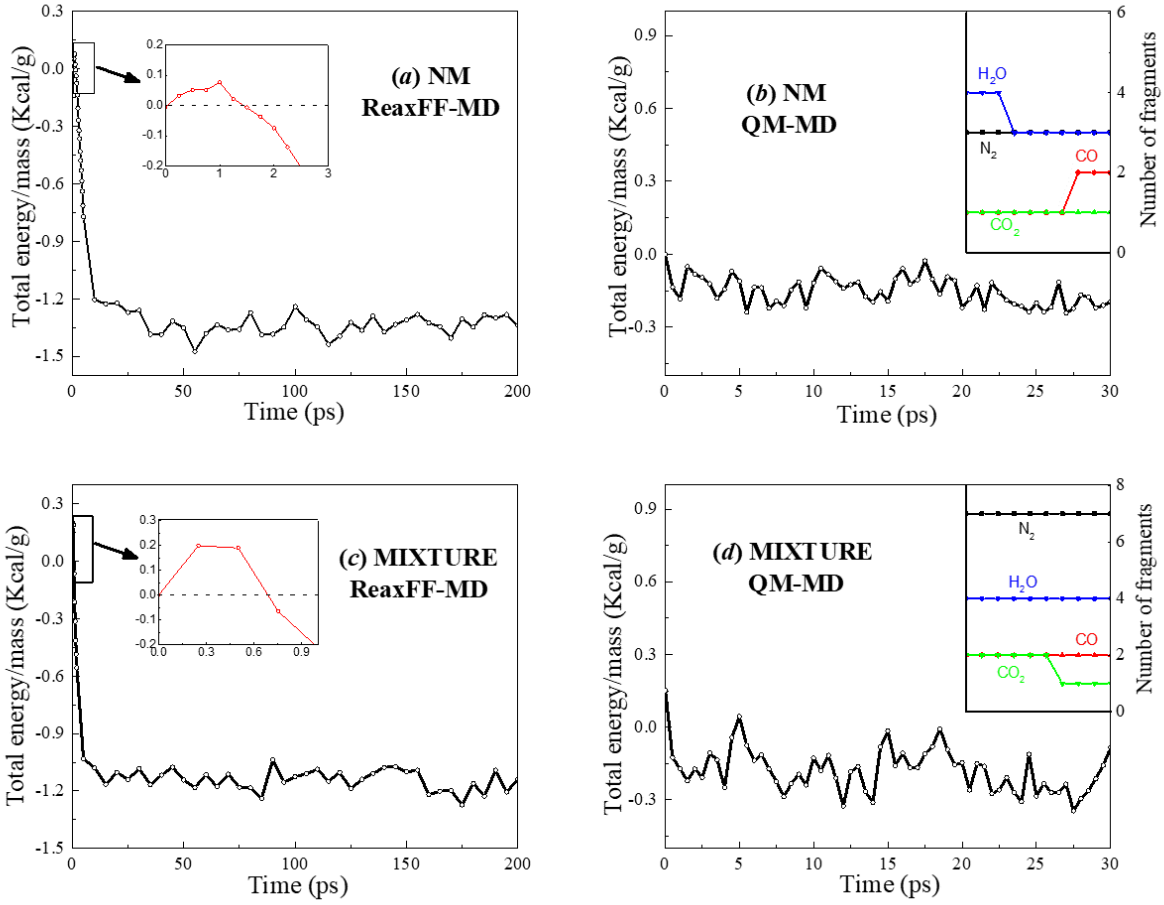

Figure 2. Time evolution of the total energy per unit mass for NVT simulations of NM and the NM-$NCCO_2$ mixture. The initial energy is set to zero as a reference. (a) RMD for the first 200 ps (inserted for the initial 3 ps) and (b) QMMD for the last 30 ps (inserted for the last 10 ps products distributions) at T = 3400 K and V/V_0 = 0.65 for the NM system. (c) RMD for the first 200 ps (inserted for the initial 1 ps) and (d) QMMD for the last 30 ps (inserted for the last 10 ps products distribution) at T = 4700 K and V/V_0 = 0.65 for the mixture system.

A family of five isotherms are obtained by repeating the long cook-off simulation for 25 times at five different temperatures with five different volume-compression-ratios for each temperature. The isotherms are spline fitted for NM, the mixture and the compressed NM systems, as shown in Figure 3. The intersection between each isotherm and the H_g = 0 axis is the exact location of the point in the fully reacted Hugoniot curve. Next we extracted the temperature and density information of these positions and carried out further cook-off simulations to determine the detonated Hugoniot curve.

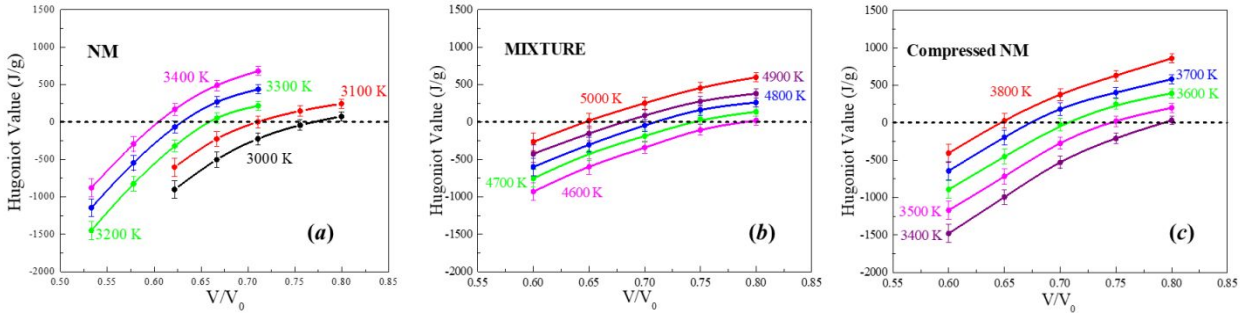

Figure 3. Spline fitted curves of the Hugoniot value and the volume-compression-ratios at various temperatures for the NM (a), the mixture (b) and the compressed NM systems (c), respectively. The fully reacted Hugoniot states are determined by the intersections of the Hg = 0 line (the dashed line) and the isotherms.

Finally, five points are fitted to a quadratic polynomial to describe the detonated Hugoniot curve, showing the pressure evolution as a function of density for the final states, as shown in Figure 4. The CJ point is located by the tangential point between the Rayleigh line and the Hugoniot curve. Thus, we obtained the CJ points at V/V_0 = 0.715 for NM, V/V_0 = 0.735 for the mixture and V/V_0 = 0.732 for the compressed NM system, respectively. In addition, the CJ temperature is derived by the quadratic polynomial fitted equation of temperature and volume compression ratio. For the NM system, the predicted properties from RMD with QMMD method are listed in Table 1. Herein, the detonation properties are obtained from the CJ state which is the fundamental chemical equilibrium state at the end of the reaction zone. The results of a very recent experimental study describing the CJ state are also listed in the table as the reference[3]. The predicted detonation properties from our simulation are D_{CJ} = 6.182 ± 0.266 km/s, T_{CJ} = 3073 ± 231 K, and P_{CJ} = 13.07 ± 1.15 GPa at ρ_0 = 1.20 g/cm^3 for NM, in good agreement with this experimental data of D_{CJ} = 6.2 km/s T_{CJ} = 3430 ± 240 K, and P_{CJ} = 11.2 GPa at ρ_0 = 1.14 g/cm^3.

In fact, uncertainties due to subjective or objective issues, as mentioned in the previous studies[2,28,29], make it difficult to capture the accurate CJ pressure of NM. For example, a slow approach to reach steady shock wave, a long reaction zone tail and a pulsating instability are interferential factors to accurately identify the CJ state from the reaction-zone profile in

experiments. Also, the equilibrium composition for the equations of states (EOS) varies among different simulations leads to different detonation pressure, such as 10.34 GPa reported by Menikoff *et al*., 11.4-13.2 GPa by Bouyer *et al*., and 12.5 GPa by Dattelbaum *et al*.

Similarly, uncertainties for the temperature inference can arise from pyrometry with the assumption of gray body radiation distribution and the absorption in the reaction zone, leading to measurements of complex inhomogeneous temperature distributions that are strongly biased toward the hottest part of the von Neumann spike (VNS) region instead of the CJ region. The reported detonation temperature is ~3600 K, but accounting for the heat absorption of carbon particles that result from the oxidization processes of nitromethane molecules would lead to a lower CJ temperature. Therefore, our first-principle descriptions of CJ state of NM are well validated by comparing with experiment[3].

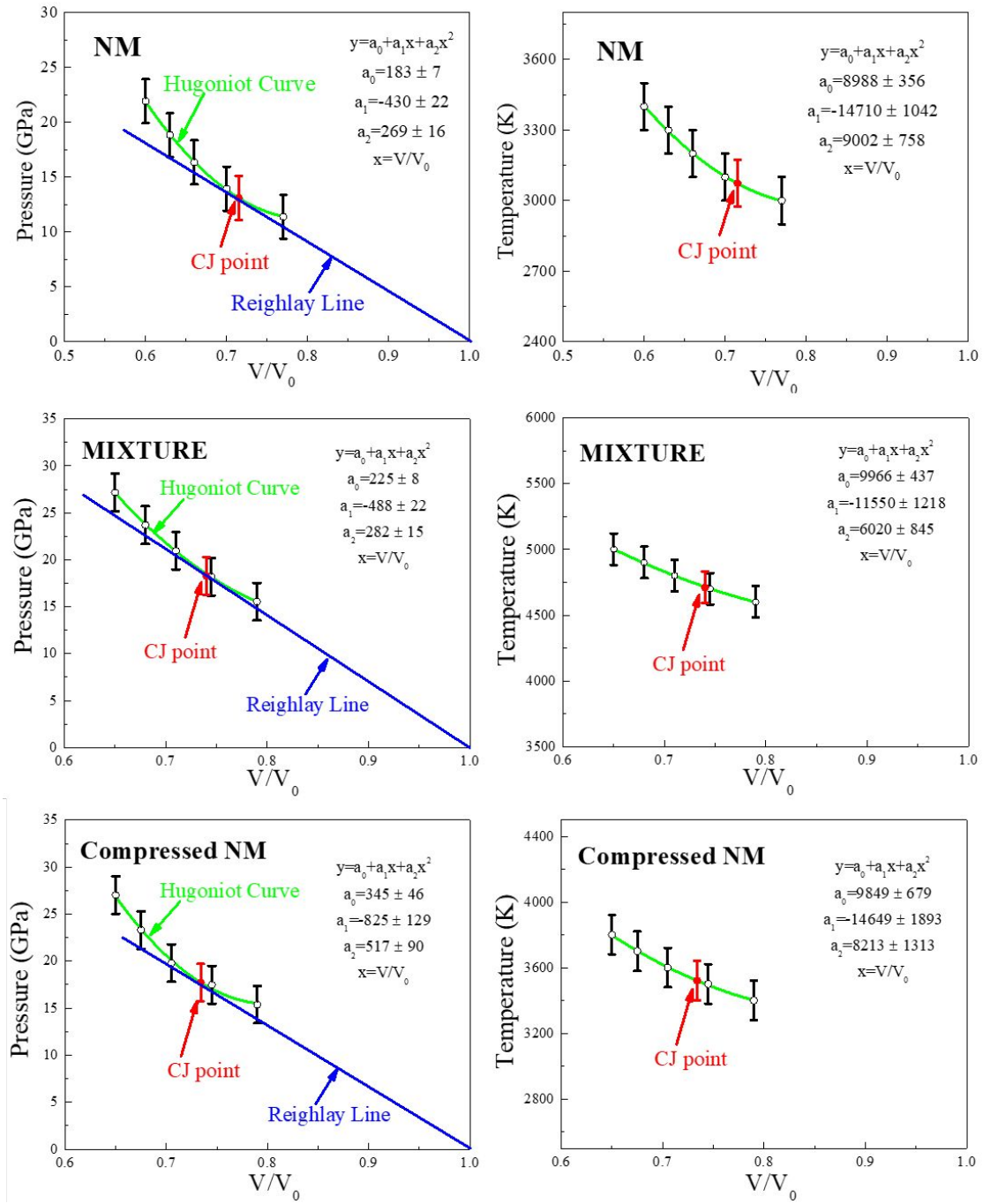

Figure 4. Hugoniot curve describing the completely detonated states, and the CJ points for NM, the mixture, and the 15% volume compressed NM. The curve of detonated temperature and compressed volume proportion satisfying $H_g = 0$. The CJ points (red dot) were derived as the tangent point of the Rayleigh line and the fully reacted Hugoniot curve.

For the mixture system, we predict the CJ temperature of $T_{CJ} = 4729 \pm 279$ K (Table 1), which is 54% higher than that of the NM system. This is because of the two nitrogen atoms contained in $NCNO_2$ molecule and the significant difference between bond strengths of 305 kJ/mol for C-N or

887 kJ/mol for C≡N in inert $NCNO_2$ molecule and 942 kJ/mol for N≡N in N_2. As a result, the decomposition of nitrogen-rich $NCNO_2$ to the corresponding final products releases an extraordinary amount of energy. In contrast, the nitrogen-poor NM molecule only has one nitrogen atom, leading to less energy output than the $NCNO_2$ molecule. Furthermore, the CJ pressure of the mixture P_{CJ} = 19.20 ± 1.27 GPa is 47% higher than that of NM system, leading to a 17% higher detonation velocity of D_{CJ} = 7.247 ± 0.235 km/s than that of NM system. **Thus, the detonation properties are greatly enhanced by adding nitrogen-rich $NCNO_2$ into the NM system.**

Table 1. Detonation properties at the CJ state for NM, mixture and compressed NM[3]

	NM			Mixture	Compressed NM
	RMD&QMMD	Exp	CHEETAH[a]	RMD&QMMD	RMD&QMMD
Density (g/cm^3)	1.20	1.14		1.38	1.38
P_{CJ} (GPa)	13.07±1.15	11.2	11.4-13.2	19.20±1.27	18.05±1.19
T_{CJ} (K)	3073 ± 231	3430 ± 240	3442-3666	4729 ± 279	3527 ± 243
V_{CJ}(cm^3/g)	0.596±0.025			0.533±0.021	0.530±0.020
D_{CJ}(km/s)	6.182±0.266	6.2		7.247±0.235	6.987±0.226

[a] The calculations with CHEETAH software varies because of using different equations of state and databases.

For the compressed NM system, we predict the CJ temperature of T_{CJ} = 3527 ± 243 K (15% higher than that of NM), the CJ pressure of P_{CJ} = 18.05 ± 1.19 GPa (38% higher than that of NM) and detonation velocity of D_{CJ} = 6.987 ± 0.226 km/s (13% higher than that of NM). This is because of more frequent and effective collisions between atoms in the dense form liquids lead to a higher temperature, while more atoms constrained in the supercell result in a higher pressure, which further increases the gas expansion to delivery energy to the shock front to achieve a faster detonation velocity. Thus, the detonation performances are increased by compressing the NM into

a denser system. Since the mixture and compressed NM system have similar density, the 34% higher of CJ temperature, 6% higher CJ pressure and 4% higher detonation velocity of mixture compared to compressed NM, shows that the additional nitrogen atoms make greater contributions to the temperature and working capacity than the hydrogen atoms.

In order to understand why the mixture shows enhanced detonation properties compared to NM system, we analyzed the detonation products by averaging the last 10 ps QMMD simulations, as listed in Table 2. For all three systems, the dominant products are N_2, H_2O, CO, and CO_2. For the mixture system, more final products (0.58 ± 0.00 mol/mol N_2, 0.33 ± 0.00 mol/mol H_2O, 0.17 ± 0.00 mol/mol CO, and 0.14 ± 0.01 mol/mol CO_2) are found than those (0.33 ± 0.00 mol/mol N_2, 0.17 ± 0.00 mol/mol H_2O, 0.16 ± 0.01 mol/mol CO, and 0.09 ± 0.01 mol/mol CO_2) in the NM system. This explains the high CJ temperature of the mixture system as due to large amounts of energy released while forming final products. Moreover, fewer atoms are trapped into small carbon clusters in the mixture system. For example, 75% C and 25% N atoms are contained in the carbon clusters in NM, compared to only 69% and 9% N atoms trapped in the mixture system. Since, more gaseous products are formed in the mixture system, CJ pressure and detonation velocity are increased. In addition, compared with NM system, no HO, fewer H and more water molecule appear in the mixture at the CJ state, indicating that hydrogen atoms tend to form isolated particles (H and HO) in hydrogen-rich NM system but form stable molecules (H_2O molecule) in hydrogen-poor mixture system. For the compressed NM system, a slightly increased amount carbon clusters are found, indicating that high pressure is helpful to form carbon aggregates, which were also observed in our previous studies[22]. These clusters will decompose and produce additional CO_2 and CO products after expansion.

Table 2. Detonation products predicted at the CJ state for NM, mixture and compressed NM

		NM	Mixture	Compressed NM
		MD&QMMD	MD&QMMD	MD&QMMD
Density (g/cm^3)		1.20	1.38	1.38
Main Products	N_2	0.33±0.00	0.58±0.00	0.25±0.00
(mol/mol)	H_2O	0.17±0.00	0.33±0.00	0.24±0.02
	CO	0.16±0.01	0.17±0.00	0.13±0.02
	CO_2	0.09±0.01	0.14±0.01	0.07±0.01
	H	0.98±0.02	0.19±0.01	0.76±0.03
	HO	0.34±0.02		0.17±0.01
Other molecules (mol/mol)				
number carbon gases		0.47±0.03	0.27±0.04	0.36±0.01
composition		$H_{0.17}N_{0.08}O_{0.15}$	$H_{0.15}N_{0.13}O_{0.04}$	$C_{0.08}H_{0.17}N_{0.54}O_{0.10}$
carbon clusters		0.58±0.06	0.50±0.09	0.64±0.11
composition		$C_{0.75}H_{0.28}N_{0.25}O_{0.42}$	$C_{0.69}H_{0.28}N_{0.09}O_{0.57}$	$C_{0.80}H_{0.39}N_{0.33}O_{0.56}$

4. CONCLUSION

In summary, we combined ReaxFF MD and QMMD simulations to examine the detonation properties of liquid NM and the 1:1 NM-$NCNO_2$ mixture. We found that the detonation properties are significantly improved by adding $NCNO_2$ into the NM system, with the CJ temperature is 54% higher than that in the pure NM system. This is because more nitrogen atoms are contained in $NCNO_2$ molecule than in NM molecule, leading to more energy to be released during the decomposition of $NCNO_2$. The CJ pressure of the mixture system is 47% higher, leading to a 17% higher detonation velocity than those of pure NM. The reason is that more gaseous final products of N_2, H_2O, CO, and CO_2 and less carbon clusters are found in the mixture system than those in the NM system. Our findings suggest that $NCNO_2$ is a promising additive or a suitable replacement

of liquid NM under low temperature conditions to enhance the detonation properties. We also compared the normal NM, with increased density NM, finding that detonation properties are increased because a more compression leads to more intense atomic interactions and higher gas expansion capability.

AUTHOR INFORMATION

Corresponding Authors: *E-mail: qia@unr.edu, wag@caltech.edu

ORCID

Dezhou Guo: 0000-0003-2094-9195

William A. Goddard III: 0000-0003-0097-5716

Qi An: 0000-0003-4838-6232

The authors declare no competing financial interests.

ACKNOWLEDGMENTS

This work is supported by the American Chemical Society Petroleum Research Fund (PRF# 58754-DNI6).

SUPPORTING INFORMATION

The Supporting Information (SI) is available free of charge on the ACS Publications website at DOI:xxx. The SI includes the Figure S1 that displays the radial distribution function of the NM-$NCNO_2$ mixture system at 273 K.

REFERENCES

1. Shrestha, K. P.; Vin, N.; Herbinet, O.; Seidel, L.; Battin-Leclerc, F.; Zeuch, T.; Mauss, F. Insights into nitromethane combustion from detailed kinetic modeling-pyrolysis experiments in jet-stirred and flow reactors. *Fuel* **2020**, *261*, 116349.

2. Menikoff, R.; Shaw, M. S. Modeling detonation waves in nitromethane. *Combust. Flame* **2011**, *158*, 2549-2558.

3. Bhowmick, M.; Nissen, E. J.; Dlott, D. D. Detonation on a tabletop: nitromethane with high time and space resolution. *J. Appl. Phys*. **2018**, *124*, 075901.

4. Campbell, A. W.; Davis, W. C.; Travis, J. R. Shock Initiation of Detonation in Liquid Explosives. *Phys. Fluids* **2018**, *4*, 498-510.

5. Nunziato, J. W.; Kennedy, J. E.; Hardesty, D. R. The thermal ignition time for homogeneous explosives involving two parallel reactions. *Combs. Flam.* **1977**, *29*, 265-268.

6. Dold, J. W.; Kapila, A. K. Comparison between shock initiations of detonation using thermally-sensitive and chain-branching chemical models. *Combs. Flam.* **1991**, *85*, 185-194.

7. Yoo, C. S.; Holmes, N. C.; Souers, P. C. Detonation in shocked homogeneous high explosives. *Mat. Res. Soc. Symp. Proc*. **1996**, *418*, 397–406.

8. Mochaloval, V.; Utkin, A.; Lapin, S. Detonation properties of nitromethane/diethylenetriamine solution. *AIP Conf. Proc.* **2015**, 1793, 030005.

9. Sheffield, S. A.; Engelke, R.; Alcon, R. R. In-situ study of the chemically driven flow fields in initiating homogeneous and heterogeneous nitromethane explosive. In *Ninth Symposium (International) on Detonation*; Office of the Chief of Naval Research 113291-7: Arlington, VA, 1989; pp 39-49.

10. Rahm, M.; Bélanger-Chabot, G.; Haiges, R.; Christe K. O. Nitryl cyanide, $NCNO_2$. *Angew. Chem. Int. Ed.* **2014**, *53*, 6893 –6897.

11. Zhang, L.; Zybin, S. V.; van Duin, A. C. T.; Dasgupta, S.; Goddard, W. A. III; Kober, E. M. Carbon cluster formation during thermal decomposition of octahydro-1,3,5,7-tetranitro-1,3,5,7-tetrazocine and 1,3,5-triamino-2,4,6-trinitrobenzene high explosives from ReaxFF reactive molecular dynamics simulations. *J. Phys. Chem. A*, **2009**, *113*, 10619–10640.

12. Rom, N.; Zybin, S. V.; van Duin, A. C. T.; Goddard, W. A. III; Zeiri, Y.; Katz, G.; Kosloff, R. Density-dependent liquid nitromethane decomposition: molecular dynamics simulations based on ReaxFF. *J. Phys. Chem. A*, **2011**, *115*, 10181–10202.

13. Zhou, T.; Zybin, S. V.; Goddard, W. A. III; Cheng, T.; Naserifar, S.; Jaramillo-Botero, A.; Huang, F. Predicted detonation properties at the Chapman-Jouguet state for proposed energetic materials (MTO and MTO_3N) from combined Reaxff and quantum mechanics reactive dynamics. *Phys. Chem. Chem. Phys*. **2018**, *20*, 3953−3969.

14. Guo, D.; Guo, D.; Huang, F.; An, Q. Influence of silicon on the detonation performance of energetic materials from first-principles molecular dynamics simulations. *J. Phys. Chem. C* **2018**, *122*, 24481-24487.

15. Momma, K.; Izumi, F. VESTA 3 for three-dimensional visualization of crystal, volumetric and morphology data. *J. Appl. Crystallogr*. **2011**, *44*, 1272-1276.

16. Kresse, G. Ab Initio molecular dynamics for liquid metals. *J. Non-Cryst. Solids* **1995**, *192-193*, 222-229.

17. Kresse, G.; Furthmüller, J. Efficiency of ab-Initio total energy calculations for metals and semiconductors using a plane-wave basis set. *Comput. Mater. Sci*. **1996**, *6*, 15−50.

18. Grimme, S.; Ehrlich, S.; Goerigk, L. Effect of the damping function in dispersion corrected density functional theory. *J. Comput. Chem*. **2011**, *32*, 1456-1465.

19. Paier, J.; Hirschl, R.; Marsman, M.; Kresse, G. The Perdew-Burke-Ernzerhof exchange-correlation functional applied to the G2-1 test set using a plane-wave basis set. *J. Chem. Phys.* **2005**, *122*, 234102.

20. Kresse, G.; Joubert, D. From ultrasoft pseudopotentials to the projector augmented-wave method. *Phys. Rev. B* **1999**, *59*, 1758-1775.

21. Blöchl, P. E.; Jepsen, O.; Andersen, O. K. Improved tetrahedron method for Brillouin-zone integrations. *Phys. Rev. B* **1994**, *49*, 16223-16233.

22. Guo, D.; Zybin, S. V.; An, Q.; Goddard, W. A. III; Huang, F. Prediction of the Chapman-Jouguet chemical equilibrium state in a detonation wave from first principles based reactive molecular dynamics. *Phys. Chem. Chem. Phys*. **2016**, *18*, 2015-2022.

23. Guo, D.; An, Q. Thermal stability and detonation properties of potassium 4,4′-bis(dinitromethyl)-3,3′-azofurazanate, an environmentally friendly energetic three-dimensional metal-organic framework. *ACS Appl. Mater. Inter*. **2019**, 11, 1512-1519.

24. Plimpton, S. Fast parallel algorithms for short-range molecular dynamics. *J. Comput. Phys*. **1995**, *117*, 1-19.

25. Liu, L.; Liu, Y.; Zybin, S. V.; Sun, H.; Goddard, W. A. III. ReaxFF-lg: Correction of the ReaxFF reactive force field for london dispersion, with applications to the equations of state for energetic materials. *J. Phys. Chem. A* **2011**, *115*, 11016−11022.

26. Guo, D.; An, Q.; Goddard, W. A. III; Zybin, S. V.; Huang, F. Compressive shear reactive molecular dynamics studies indicating that cocrystals of TNT/CL-20 decrease sensitivity. *J. Phys. Chem. C* **2014**, *118*, 30202−30208.

27. Guo, D.; An, Q.; Zybin, S. V.; Goddard, W. A. III; Huang, F.; Tang, B. The co-crystal of TNT/CL-20 leads to decreased sensitivity toward thermal decomposition from first principles based reactive molecular dynamics. *J. Mater. Chem. A* **2015**, *3*, 5409−5419.

28. Bouyer, V.; Darbord, I.; Herve, P.; Baudin, G.; Gallic, C. L.; Clement, F.; Chavent, G. Shock-to-detonation transition of nitromethane: time-resolved emission spectroscopy measurements. *Combust. Flame* **2006**, *144*, 139.

29. Dattelbaum, D. M.; Sheffield, S. A.; Stahl, D. B.; Dattelbaum, A. M.; Trott, W.; Engelke, R. Influence of hot spot features on the shock initiation characteristics of heterogeneous nitromethane. *AIP Conf. Proc.* **2009,** *263*, 1195.

TOC Graphic

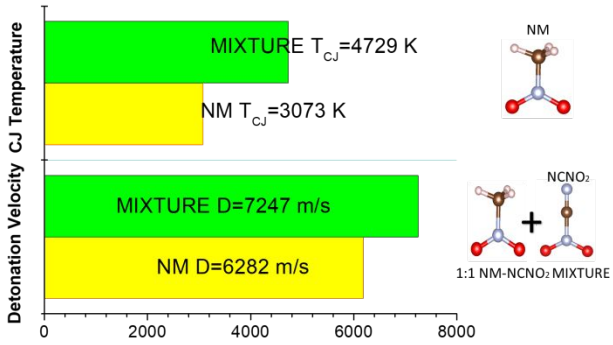
Detonation Velocity CJ Temperature
MIXTURE T_{CJ}=4729 K
NM T_{CJ}=3073 K
MIXTURE D=7247 m/s
NM D=6282 m/s
0
2000
4000
6000
8000
NM
$NCNO_2$
1:1 NM-$NCNO_2$ MIXTURE